



HAL
open science

Direct Structural Evidence for Interfacial Gradients in Asymmetric Polymer Nanocomposite Blends

Anne-Caroline Genix, Vera Bocharova, Bobby Carroll, Philippe Dieudonné-George, Michael Sztucki, Ralf Schweins, Alexei Sokolov, Julian Oberdisse

► **To cite this version:**

Anne-Caroline Genix, Vera Bocharova, Bobby Carroll, Philippe Dieudonné-George, Michael Sztucki, et al.. Direct Structural Evidence for Interfacial Gradients in Asymmetric Polymer Nanocomposite Blends. ACS Applied Materials & Interfaces, Washington, D.C.: American Chemical Society, 2021, 13 (30), pp.36262-36274. 10.1021/acsami.1c06971 . hal-03384179

HAL Id: hal-03384179

<https://hal.archives-ouvertes.fr/hal-03384179>

Submitted on 18 Oct 2021

HAL is a multi-disciplinary open access archive for the deposit and dissemination of scientific research documents, whether they are published or not. The documents may come from teaching and research institutions in France or abroad, or from public or private research centers.

L'archive ouverte pluridisciplinaire **HAL**, est destinée au dépôt et à la diffusion de documents scientifiques de niveau recherche, publiés ou non, émanant des établissements d'enseignement et de recherche français ou étrangers, des laboratoires publics ou privés.

Direct structural evidence for interfacial gradients in asymmetric polymer nanocomposite blends

Anne-Caroline Genix,^{1*} Vera Bocharova,² Bobby Carroll,² Philippe Dieudonné-George,¹ Michael

Sztucki,³ Ralf Schweins,⁴ Alexei P. Sokolov,^{2,5} and Julian Oberdisse¹

¹Laboratoire Charles Coulomb (L2C), Université de Montpellier, CNRS, F-34095 Montpellier, France

²Chemical Sciences Division, Oak Ridge National Laboratory, Oak Ridge, TN 37831, USA

³European Synchrotron Radiation Facility, 71 Avenue des Martyrs, CS 40220, F-38043 Grenoble Cedex 9, France

⁴Institut Laue-Langevin, DS/LSS, 71 Avenue des Martyrs, CS 20156, F-38042 Grenoble Cedex 9, France

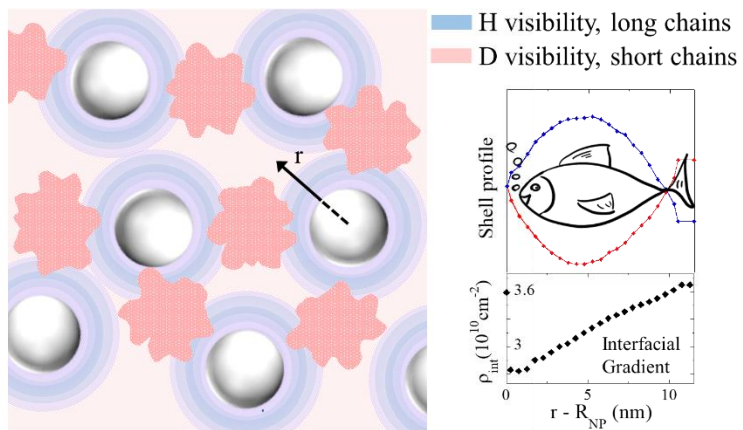
⁵Department of Chemistry, University of Tennessee, Knoxville, TN 37996, USA

* Corresponding author: anne-caroline.genix@umontpellier.fr

Abstract. Understanding the complex structure of polymer blends filled with nanoparticles (NPs) is the key to designing their macroscopic properties. Here, the spatial distribution of hydrogenated (H) and deuterated (D) polymer chains asymmetric in mass is studied by small-angle neutron scattering. Depending on the chain mass, a qualitatively new large-scale organization of poly(vinyl acetate) chains beyond the random-phase approximation is evidenced in nanocomposites with attractive polymer-silica interactions. The silica is found to systematically induce bulk segregation. Only with long H-chains, a strong scattering signature is observed in the q -range of the NP size: it is the sign of interfacial isotopic enrichment, i.e., of contrasted polymer shells close to the NP surface. A quantitative model describing both the bulk segregation and the interfacial gradient (over ca. 10 – 20 nm depending on the NP size) is developed, showing that both are of comparable strength. In all cases, NP surfaces trap the polymer blend in a non-equilibrium state, with preferential adsorption around NPs only if chain length and isotopic preference towards the surface combine their entropic and enthalpic driving forces. This structural evidence for interfacial polymer gradients will open the road to quantitative understanding of the dynamics of many-chain nanocomposite systems.

Keywords: interfacial segregation, polymer nanocomposites, isotopic polymer blends, chain-mass asymmetry, small-angle scattering, low- q upturn, concentration fluctuations.

GRAPHICAL ABSTRACT:



INTRODUCTION

Polymer nanocomposites (PNCs) made by incorporating hard filler nanoparticles (NPs) into polymer melts have striking structural and dynamical properties which depend in a subtle way on interactions between the chains and the particle surfaces, and on entropic effects related to the configuration and distribution of chains close to the NPs. For strongly interacting systems like poly(vinyl acetate)/silica where hydrogen bonds form between the carbonyl groups and the silanols,¹ such properties have been deeply investigated by scattering experiments – showing the existence of depleted polymer zones² – and most importantly, broadband dielectric spectroscopy (BDS) evidencing the existence of *slowed-down* regions in the sample.^{1,3-4} In weakly interacting PNCs like filled elastomers, BDS and NMR evidenced a weak impact on dynamics with a slight broadening of the segmental time distribution⁵ and a low fraction of slowed-down polymer,⁶⁻⁷ respectively. In a similar way, recent quasi-elastic neutron scattering experiments revealed only a small slowing down of the self-dynamics well-above the glass-transition temperature.⁵

In order to shed light onto the peculiar behavior of PNCs and chain microstructure, small-angle neutron scattering (SANS) is a method of choice.⁸ Mixing of hydrogenated (H) and deuterated (D) chains in blends is generally used to either highlight chain conformation explored with SANS experiments,⁹ or in order to match the scattering contribution of other constituents of the material, like the one of NPs within polymer nanocomposites.¹⁰⁻¹¹ The latter method, called zero-average contrast (ZAC),¹² allows following concentration fluctuations of the isotopes, which may reflect single chain conformations, or local enrichment of chains in some region of the samples. Here, we study isotopic blends of chemically identical chains of different mass, in presence of nanoparticles.

The thermodynamics of chain mixing is usually described with the mean-field Flory-Huggins formalism.¹³ A positive monomer interaction parameter χ expresses the propensity of a binary melt to demix for enthalpic reasons, an effect which is counterbalanced by the mixing entropy of the chains. Within the random phase approximation (RPA) by de Gennes,¹⁴ the neutron scattered intensity of fluctuations in the homogeneous state can be calculated in a mean-field approximation based on the chain form factors and χ , and it is found to diverge at low q for $\chi > \chi_c$. This divergence indicates the onset of demixing at the so-called “neutron cloud point”.¹⁵ When the T-dependence of χ makes it cross χ_c , a critical solution temperature is met, defining the spinodal curve in a Φ -T phase diagram. This curve subdivides the miscibility gap into a metastable region up to the binodal, and an unstable region of spinodal decomposition.¹⁶ The critical parameter χ_c is directly related to the number of monomers per chain and this value is lower for a blend of long chains, thus favoring phase separation, with a diverging correlation length. Beyond this critical point, the mean-field theory fails because it considers only the

average environment of a monomer, and ignores large-scale concentration fluctuations,¹⁷⁻¹⁸ the growth kinetics of which usually follows the Cahn-Hilliard theory.¹⁹

For polymeric systems, the formation of growing bicontinuous and locally periodic (spinodal) structures has been evidenced since the 1970s.²⁰⁻²¹ Recently, Cabral and Higgins have highlighted experimental and theoretical studies of spinodal decomposition in polymer blends, focusing on its growth dynamics.²² Inoue et al have shown that the jump into the spinodal region of a solution-cast polymer blend by drying is both speed and polymer mass-dependent, and that once created, spinodal structures may be frozen.²³ In the metastable region, nucleation and growth is the dominant mechanism, but again the polymeric nature of these systems may lead to a high energy barrier for nucleation, and possibly freeze any structure.¹⁷ The temperature-dependence of decomposition has also been studied by SANS and isotopic labeling, allowing comparison to the Ginzburg-Landau approach of phase transitions, and identifying the limits of the mean-field theories.²⁴⁻²⁵ The phase diagrams of pure blends are thus relatively well-described by mean-field theories of known limitations. On the other hand, the effect of the introduction of NPs on the phase behavior is weak and system-dependent as shown by a few phenomenological theories²⁶⁻²⁹ and measurements.³⁰⁻³² Ginzburg²⁶ predicted the effect of nanoparticles on the phase separation of PNC blends. He showed in particular that a possible enthalpic compatibilizing effect of NPs is counterbalanced for larger particles ($R_{NP} > R_g$ of the chain) by the entropic penalty on the chain conformation.

In this article, the question of concentration fluctuations close to NP surfaces in isotopic chain blends is addressed for various degrees of polymerization, including symmetric and asymmetric blends. This is motivated by the observation of dynamical heterogeneities in attractive PNCs where interfacial layers of different – slowed-down – segmental dynamics with respect to the bulk and extending over 2–6 nm around the NPs have been characterized by BDS. A strong impact of chain mass has been established, the short chains displaying lower relaxation times in the interphase.³³⁻³⁴ This effect has been ascribed to a MW-dependent chain packing in the interfacial layers with a reduction in mass density for the long chains confined between neighboring particles. Such a reduction is obviously disadvantageous for the mechanical properties of high-MW PNCs, but it could be counterbalanced by chain stretching which prevails for long chains. Following this idea, binary blends of otherwise the same short and long chains have been recently studied showing that the presence of a small fraction of short chains leads to an improved mechanical reinforcement.³⁵ Swelling of the interface with the short chains tends to favor stretching of the long chains as deduced from molecular dynamics simulations. This behavior motivated our study of PNCs with asymmetric blends.

In order to understand the formation of polymer structures, one must keep in mind the formulation pathway of such systems, which are usually obtained by evaporation after mixing in solvents. It is well-known that most of the mobility is available only in presence of solvent, thus quenching chain conformations in the dry and glassy state,³⁶ e.g., during neutron scattering experiments³⁷. In true homopolymer melts and solutions of chains of different mass close to surfaces, there are no enthalpic reasons besides chain-end corrections for one or the other chain to be attracted to the surface. In this case, the lower reduction in translational entropy caused by locating a chain close to the surface favors the adsorption of the longer chains.³⁸ The isotopic difference between H- and D-chains used in neutron scattering causes a small energetic preference. Due to differences in the bond length (C-D vs C-H) and thus electronic polarizability,³⁹ isotopic polymer mixtures are not ideal systems and possibly phase separate⁴⁰ depending on the temperature as described above. An excess low-q scattering has been observed by SANS and associated with finite-size domains indicating that H/D blend can also be trapped in a metastable state.⁴¹ Small differences in surface energy also lead to surface-driven phase separation. Deuterated segments display a lower surface energy and systematically enrich the air surface in symmetric polymer blends.⁴²⁻⁴⁴ However, it has been shown that entropic factors may overcome the energetic interactions in mixtures of short and long chains.⁴⁵ This behavior points out the importance of chain-length disparity in blends regarding surface segregation, the reproduction of which requiring the inclusion of compressibility effects.⁴⁶ In presence of silica, isotopic substitution may thus affect interactions with surface silanols and cause a weak enthalpic preference of one type of chain for the particle surfaces. This argument has been used by Jouault et al¹¹ as a possible explanation for the H/D chain separation triggered by silica NPs in symmetric polystyrene (PS) blends. However, such effects are usually weak and they do not impact chain conformations in PNCs, as shown by the tremendous efforts devoted to the measurement of the chain radius of gyration in PNCs over the last 20 years.^{10-11, 47} As a result, depending on the difference in mass between the long and the short chains and their energetic preference, the enthalpic and entropic driving force towards the NP surface may either compensate or reinforce each other – the latter namely in the case where the longer chains are attracted to the surface. This mechanism might then destabilize the large-scale distributions of the chains, and trigger new isotopic contrast situations, which in turn should be visible in SANS experiments. Such a situation was encountered in PNCs by Crawford et al who observed an excess scattering attributed to the onset of phase separation in presence of silica, without quantitatively describing it.⁴⁷ Unexplained low-q upturns are commonly encountered in PNCs, and their description is one of the objectives of the present paper. Effects of particles on the polymer correlations may induce a low-q increase. At high filler fractions and increasing interfacial attraction, large-scale heterogeneities that may be associated with “polymer-mediated bridging” are precursor of spinodal decomposition with a noticeable low-q increase in the polymer structure factor.⁴⁸ In addition

to the upturn, a structure factor peak at intermediate q has been observed and backed up by theoretical work in the framework of the polymer reference interaction site model (PRISM).⁴⁸⁻⁵¹ Both aspects will be discussed with our results.

The aim of this article is to investigate the large-scale distribution of polymer isotopes in PNCs, which appear to be induced by the presence of the NPs, but remain quenched after PNC formation. As a starting point, the pure blends of different chain asymmetry will be studied. Then, striking differences in behavior as NPs are added to different matrices will be evidenced, and modeled by two types of large-scale geometric structures: one describes isotropic fluctuations triggered by the presence of the NPs, but distributed independently of the filler particles throughout the matrix. And the second one is the surprising formation of isotopic shells surrounding the silica. Such large-scale structures escape any description by the above-mentioned mean-field theories, and indeed they do not show the characteristic low- and intermediate- q shapes proposed by RPA, but rather display qualitatively new large-scale organization beyond mean field. Our results highlight the surprisingly asymmetric behavior of isotopic blends with respect to chain length close to NPs, and it is hoped to open the road to understanding the puzzling dynamical properties of polymer blends filled with nanoparticles.

RESULTS AND DISCUSSION

Pure blends. Samples were formulated by mixing hydrogenated and deuterated poly(vinyl acetate) (PVAc) (Table 1) in solvent before drying, with the samples named HX (hydrogenated) or DX (deuterated), where X indicates the molecular weight in kg/mol (e.g., D40 for a deuterated 40 kg/mol chain). The scattered intensity of pure H and D blends (i.e., without NPs) is caused by the local isotopic fluctuations representative of the chain conformations. The standard description following the random phase approximation gives the intensity $I_{\text{RPA}}(q)$ as a sum of three terms, one for each form factor $P_i(q)$, with $i = \text{H}$ or D , and a third term taking the monomeric interaction χ into account⁵²

$$\frac{\Delta\rho^2}{I_{\text{RPA}}(q)} = \frac{1}{\Gamma_{\text{H}} N_{\text{H}} V_{\text{H}} P_{\text{H}}(q)} + \frac{1}{\Gamma_{\text{D}} N_{\text{D}} V_{\text{D}} P_{\text{D}}(q)} - \frac{2\chi}{V_0} \quad (1)$$

The chain form factor $P_i(q)$ depends on $R_g^{(i)}$, the radius of gyration of each type of chain, and N_i and V_i are the weight-average number of monomeric units per chain, and monomeric unit volume. $V_0 = \Gamma_{\text{H}}V_{\text{H}} + \Gamma_{\text{D}}V_{\text{D}}$ is the average monomer volume calculated with the volume fraction of H (resp. D) chains within the matrix, Γ_{H} (resp. Γ_{D}). In melts, the form factor of ideal Gaussian H or D-chains $P_{\text{chain}}(q)$ is given by the Debye equation:

$$P_{\text{chain}}(q) = \frac{2}{q^4 R_g^4} \left(\exp(-q^2 R_g^2) - 1 + q^2 R_g^2 \right) \quad (2)$$

In Figure 1, the scattered intensity of a symmetric blend of short chains H10/D10 is shown. At high and intermediate q , the scattering curve is perfectly described by the combination of eqs. (1) and (2), with a virtually identical radius of gyration of $R_g^{(i)} = 3.1$ nm for H- and D-chains. The exact chain masses have been determined by size-exclusion chromatography (SEC) – see Table 1 – and they have been taken into account as indicated below. The successful description shows that the H- and D-chains are mixed on a molecular level. Nonetheless, an upturn is observed at small angles. We have tentatively taken the Flory-Huggins interaction term in eq. (1) into account, for H10/D10 and many other matrices, spanning the entire mass range as given in Table 1.

Table 1. Characteristics of the hydrogenated (H) and deuterated (D) PVAc. Mw is the weight-average molecular weight and PI the polydispersity.

| Name | Mw (kg/mol) | PI | R_g (nm) |
|------|-------------|-----|------------|
| D10 | 10.4 | 1.2 | 3.1 |
| H10 | 10.2 | 1.2 | 3.1 |
| H20 | 19.6 | 1.3 | 4.3 |
| D40 | 39.6 | 1.3 | 6.1 |
| H40 | 43 | 1.4 | 6.3 |
| H110 | 113 | 1.3 | 10.2 |
| H240 | 242.7 | 2.7 | 15.0 |

The monomer-interaction term is found to stay below $\chi = 2 \cdot 10^{-3}$ for all matrices, and choosing $\chi = 0$ is consistent with all intensities reported here. These pure isotopic polymer blends thus display ideal and homogeneous chain mixing. We found that the low- q upturn observed in Figure 1 cannot be described by RPA, and that it is much weaker than the upturns related to large-scale isotopic concentration fluctuations in presence of silica presented below. This feature must be attributed to voids and defects typical of polymer melts.^{10, 53} In order to avoid artefacts induced by the very small-angle scattering in all the fitting procedures in this article, we have thus chosen to first favor fits of the intermediate and high- q range, and only afterwards optimize the available low- q scattering as much as possible in presence of NPs.

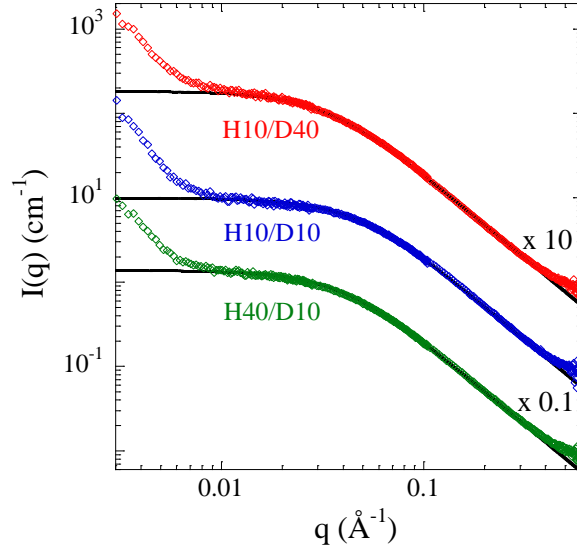


Figure 1. Scattered intensity of pure symmetric H10/D10 ($\alpha \approx 1$) and two asymmetric blends (H10/D40, $\alpha = 0.26$, vertically shifted $\times 10$; H40/D10, $\alpha = 4.1$, vertically shifted $\times 1/10$), compared to the RPA fit with $\chi = 0$ corresponding to the average of the Debye form factors with parameters given in Table 1.

In order to describe asymmetric blends of different chain mass, the radius of gyration of chains of different masses has been parametrized using the Gaussian chain statistics:

$$R_g^{(i)} = 0.9636 M w_i^{1/2} \quad (3)$$

where the weight-average chain mass $M w_i$ is given in kg/mol, and $R_g^{(i)}$ in nm. The numerical prefactor results from a simultaneous optimization of the scattering from blends combining all chain masses reported in Table 1, ranging from 10 – as shown in Figure 1 – to ca. 250 kg/mol (see SI for additional scattering of blends). In practice, it leads to a reduction of the number of fit parameters in eq. (1), as chain scattering is now perfectly known. For the rest of this article, we can thus concentrate on the analysis of the low and intermediate q -range. For comparison, the case of asymmetric matrices (H10/D40, and its inverse H40/D10) has been superimposed in Figure 1, with intensities shifted vertically for clarity. As asymmetric matrices play an important role in this article, we define the matrix asymmetry parameter α as follows:

$$\alpha = M w_H / M w_D \quad (4)$$

where the weight-averaged masses have been used. The description at intermediate and high q of the samples $\alpha = 0.26$ and $\alpha = 4.1$ in Figure 1 using eqs. (1-3) with $\chi = 0$ is equally satisfying as with α close to 1. This indicates that in all the reported cases blending hydrogenated and deuterated PVAc chains is favorable in absence of silica NPs. As with the symmetric blend, a similar low- q upturn, which is thus independent of chain mass, is observed in both asymmetric cases.

Nanocomposites. Having characterized both symmetric and asymmetric silica-free blends, and found no signs of incompatibility, we can now investigate the effect of the presence of NP surfaces on the polymer structure (see section 4 for the PNC formulation). Our rationale is that differences observed in dynamics have been related to the presence of polymer surface layers with different properties than the bulk, like a different composition in terms of chain mass,³⁵ or a different mass density close to the surface.² The latter very subtle effect has been revealed by a SAXS analysis, and it will be shown below that it is too weak to affect our SANS data. The first effect, however, would be reflected in our experiments by a different isotopic composition, and should lead to signatures visible in SANS. In order to check the influence of the amount of available surface, two silica beads of different size have been used. The corresponding form factors are well-described by a log-normal distribution of spherical objects with a radius of $R_{NP} = 9.4$ nm (log-normal polydispersity 17%), and 21.2 nm (12%), respectively as shown in SI. Their scattering length density has been determined by independent contrast variation experiments reported in² and in the SI: $\rho_{NP} = 3.59$ (resp. 3.63) 10^{10} cm^{-2} for small (resp. big) NPs, indicating similar density. The spatial distribution of NPs in nominally identical PNCs has been investigated previously² showing the formation of zones slightly denser than the average for PNC blends of low chain mass, whereas a homogeneous (non-aggregated) hard-sphere dispersion was found at the highest masses. We now compare the polymer structure in pure H/D blends to nanocomposites made with the same blends. We note that the R_g of the chains is of the same order of magnitude as the silica particle size (i.e., neither protein nor colloid limiting case), which according to Ginzburg²⁶ may make the system more prone to phase separation.

In order to highlight the polymer contribution using the ZAC-technique, PNC samples have been designed in such a way that the average contrast of the silica NPs is always zero^{10,12}

$$\Delta\rho_{NP} = \rho_{NP} - \rho_{mat} = \rho_{NP} - (\Gamma_H \rho_H + \Gamma_D \rho_D) = 0 \quad (5)$$

with the chain volume fractions obeying $\Gamma_H + \Gamma_D = 1$. For the two silica beads, Γ_H is found to be ca. 60%, see SI for exact values used in all calculations. As indicated in eq. (5), the scattering length density of the matrix ρ_{mat} is given by the volumetric average of the H and D chains in the matrix with $\rho_H = 1.38$ 10^{10} cm^{-2} , and $\rho_D = 7.02$ 10^{10} cm^{-2} as determined in². The intensity scattered by a nanocomposite in the same symmetric matrix as in Figure 1 (H10/D10, $\alpha \approx 1$) with $\Phi_{NP} = 6.9$ %v of small silica NPs (Figure 2a) shows that matching is quite perfect: indeed, no contribution of the silica form factor with its high-q oscillations – as measured independently by SAXS and shown in SI – is observed.

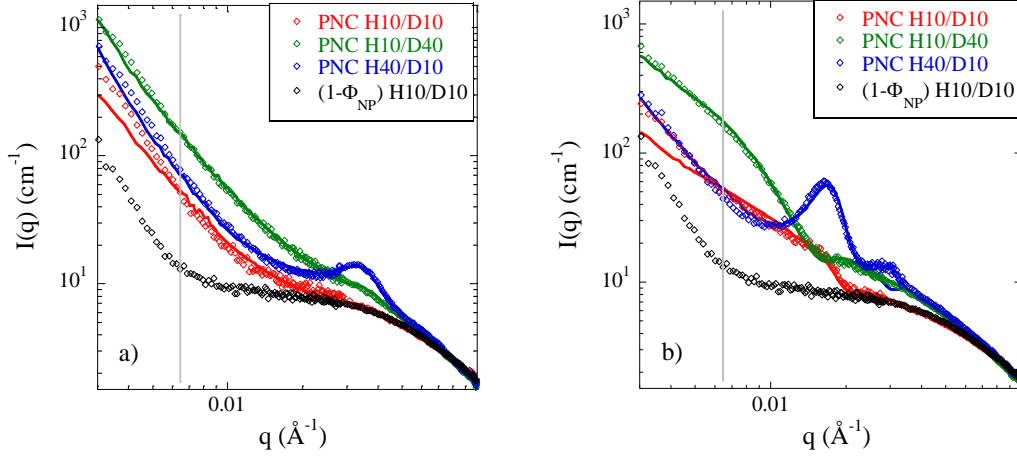


Figure 2. Scattered SANS intensity of PNCs with symmetric H10/D10 ($\alpha \approx 1$) and asymmetric blends (H10/D40, $\alpha = 0.26$ and H40/D10, $\alpha = 4.1$), for **(a)** small silica NPs, and **(b)** big silica NPs, $\Phi_{NP} \approx 8\%$. Pure matrix scattering is shown for comparison (black symbols). Chain scattering is described by RPA using the Debye form factor, cf. the text for the complete model leading to the fits superimposed to the data (solid lines).

The SANS intensity looks like the one observed in Figure 1 and superimposed in Figure 2 for the symmetric matrix for comparison, with a perfect description of the chain scattering in terms of the Debye function providing the radius of gyration and the ideal chain conformation: $R_g = 3.1$ nm given by eq. (3), as in the pure melt. H- and D-chains thus continue mixing on a molecular level. In Figure 2, the position of the upturn in the pure polymer blend has been indicated by the vertical line for illustration of the low- q domain with less reliable scattering data. In spite of this feature, the low- q increase is obviously much higher in presence of NP surfaces by ca. a factor of five, and extends to higher q . This means that the formation of some large-scale structures has been triggered by the silica NPs. A stronger low- q upturn is observed in matrix with an asymmetric (H10/D40, $\alpha \approx 1/4$) composition (Figure 2a). Surprisingly, the opposite asymmetry (H40/D10, $\alpha \approx 4$) induces a new feature: a maximum in scattering at intermediate angles, around 0.035 \AA^{-1} . The structural evolution underlying these changes necessitates quantitative modeling in order to understand the new spatial distribution of the polymer isotopes. Before doing so, it is checked in Figure 2b that these observations are robust with respect to increasing the size of the silica NPs from about 20 to ca. 40 nm. The same behavior is observed as a function of matrix asymmetry, with strong low- q upturns with respect to the pure melt for $\alpha \leq 1$, and a prominent peak showing up for longer hydrogenated chains, $\alpha > 1$. It is noted that changing the NP size by a factor of two induces a corresponding shift in the peak position, suggesting that the peak is related to a change in the matrix composition close to the silica surface.

There is no signature of the silica form factor in any of the intensities plotted in Figure 2, and the stronger low- q increase must be related to the polymer, which was intended to present a homogeneous H/D mixture. Apparently, this is not the case in PNCs, and large-scale isotopic

fluctuations are observed despite molecular mixing, as if the silica surface favored H/D segregation into zones having different chain mixing ratios. We have chosen to describe this segregation by the presence of zones of isotopic composition Γ_H^{seg} different from the nominal matrix composition Γ_H entering the above definition of ρ_{mat} : $\Gamma_H^{\text{seg}} = \Gamma_H + \Delta\Gamma_H^{\text{seg}}$. The sign of the “visibility” of segregation $\Delta\Gamma_H^{\text{seg}}$ cannot be determined, lack or gain of H-chains in the segregated zones leading to a symmetric result. We thus report its absolute value $|\Delta\Gamma_H^{\text{seg}}|$. The existence of such segregated zones has two effects on the scattering: first, the zones themselves contribute to the scattering. Secondly, their isotopic enrichment contributes to a corresponding isotopic depletion of the matrix – ρ_{mat} changes due to volume conservation of H- and D-chains. This shifts the equilibrium of eq. (5), and in principle confers visibility to the NPs even if their contribution remains weak in the present case. The shape of the zones is unknown, and we described them by spheres of radius R_{seg} , which is a fit parameter related to the position of the low- q upturn in Figure 2. Moreover, we have introduced a fuzzy surface because this appears to be the expected situation, and set the fuzziness to 20% (cf. SI). Note that choosing a different fuzziness (including sharp interfaces) has no impact on the fits or the outcome of our approach: the only important feature is the total sphere mass. The last parameter to be set is the number density of these fuzzy balls representing the volume phase separation of H- and D-chains. A natural choice is to set this number equal to the number of silica nanoparticles, with the underlying idea that segregation – which is absent in the pure blends (Figure 1) – is linked to the spatial distribution of the NPs. In the SI, different choices are explored for the number density of segregated zones, which is found to be rather constrained around one fuzzy ball per silica NP. The model for the total SANS intensity with segregated zones and silica NPs thus reads:

$$I(q) = \Delta\rho_{\text{seg}}^2 \Phi_{\text{seg}} V_{\text{seg}} P_{\text{seg}}(q) S_{\text{seg}}(q) + I_{\text{Debye}}(q) + \Delta\rho_{\text{NP}}^2 \Phi_{\text{NP}} V_{\text{NP}} P_{\text{NP}}(q) S_{\text{NP}}(q) \quad (6)$$

Here the RPA expression for chain scattering in eq. (1) has been renamed I_{Debye} in order to emphasize that χ has been set to zero. Note that this expression is applied to the entire polymer material as there is no complete phase segregation. The contrast prefactors $\Delta\rho_{\text{seg}}$ and $\Delta\rho_{\text{NP}}$ have been expressed with respect to the matrix, and are based on the isotopic composition Γ_H^{seg} of the segregated zones, which in turn affects ρ_{mat} . Φ_{seg} denotes the volume fraction of the segregated zones in the sample which is given by the product of their number density and volume depending on R_{seg} and the (fixed) fuzziness. Moreover, the apparent structure factor of the silica NPs, $S_{\text{NP}}(q)$, has been obtained by division of the SAXS intensity by the average NP form factor, while the one of the segregated zones is a priori unknown. We have thus only two fit parameters in eq. (6): R_{seg} and $\Delta\Gamma_H^{\text{seg}}$, all others being fixed or recalculated by mass conservation. Note that in all cases SAXS and SANS experiments were performed on the same piece of sample.

The outcome of the fit procedure with silica, segregated zones, and matrix polymer has been superimposed to the H10/D10- and H10/D40-data in Figure 2a. Two options for the structure factor of the segregated zones have been investigated (see SI) with either uncorrelated zones ($S_{\text{seg}}(q) = 1$) or $S_{\text{seg}}(q) = S_{\text{NP}}(q)$. The description of the large-scale structure based on the silica dispersion $S_{\text{NP}}(q)$ was found to reproduce the scattering best. This is in line with the observation that the slopes of the SAXS and SANS intensities are parallel at low q . The resulting radius of the segregated zones, R_{seg} , is found to be 15.8 nm, i.e., about 1.5 times larger than the silica radius. By no means, however, can the segregation model in eq. (6) reproduce the peaked intensity of the H40/D10 PNC as discussed below for each scattering contribution. The same observations are true for the bigger NPs reported in Figure 2b. Again, the silica has almost no visibility due to only a slight violation of eq. (5), and the segregated (thus contrasted) zones are found to dominate the scattering at low and intermediate q . Note that the bigger silica NPs have a mass higher by about a factor of ten, with a corresponding decrease in the NP number density. Nonetheless, the SANS intensities of the $\alpha = 0.26$ and $\alpha = 1$ samples based again on the silica structure factor also for the segregated zones are satisfactorily described, with a radius R_{seg} again larger than R_{NP} ($R_{\text{seg}} = 23.5$ nm on average, see SI), whereas the peaked $\alpha = 4.1$ obviously needs an additional structural element.

The most surprising result of this study was triggered by the inversion of the chain asymmetry to long H-chains with short D-chains ($\alpha > 1$). As shown in Figure 2, a new feature is present in the intermediate q -range for the H40/D10 PNCs: a well-defined peak shows up, approximately towards the end of the Guinier plateau of the NPs. This feature can be rationalized by isotopic enrichment close to the silica surface leading to the formation of a contrasted polymer shell. Such a structure can create the intensity maximum, while also contributing at low- q to the intensity upturn. This peak may likely be related to the “microphase polymer peak” observed in homopolymer-based PNCs with attractive interactions. Extensive prior studies combining small-angle scattering and non-mean-field integral equation theory based on PRISM demonstrated that the partial structure factor resolving the polymer-polymer concentration fluctuations correlates with that of the silica NPs.^{48, 51, 54} The filler-induced polymer peak is located at the NP scale – as observed here – and it is due to the exclusion of polymer chains from the occupied space of correlated NPs, thus evidencing an imprinting of NP order on the adsorbed polymer layers detected. It was reported in contrast-matched SANS experiments of Kim et al.⁵⁰ for dense polymer solutions and Sen et al.⁵⁵ for symmetric isotopic PS blends in presence of silica. Note that an analogous peak in the structure factor was also reported in the phase-separated structure of binary molecular mixtures confined in a porous material.⁵⁶ In our case, the shell with local H/D deviation highlights the NP shape and makes the NPs gain additional visibility as compared to the previous case ($\alpha \leq 1$), where only bulk segregation was observed. The fits for $\alpha > 1$ in Figure 2a and 2b,

for small and big NPs, respectively, have been obtained with a model taking both the segregation and the isotopically visible shell into account.

In practice, the (third) NP term in eq. (6) is extended, now including both the NP core and the isotopic surface layer in a core-shell form factor, $P_{cs}(q)$:

$$I(q) = \Delta\rho_{seg}^2 \Phi_{seg} V_{seg} P_{seg}(q) S_{seg}(q) + I_{Debye}(q) + P_{cs}(q) S_{NP}(q) \quad (7)$$

Due to the heterogeneity with both core and shell profile, a single contrast and volume fraction do not factor out in eq. (7). They are part of the entire expression for $P_{cs}(q)$, but average values Φ_{shell} and $\Delta\rho_{shell}$ and thus the shell visibility $\Delta\Gamma_H^{shell}$ can be defined. The sign of the latter quantity is negative if one chooses a positive $\Delta\Gamma_H^{seg}$. In practice, the interface has been described by a free scattering length density profile $\rho_{shell}(r)$ ($N_p = 20$ to 40 shells of thickness $\Delta R = 5 \text{ \AA}$) extending up to the limit defined by the total silica volume fraction and the presence of the segregated volumes. Its scattering contribution $P_{cs}(q)$ reads:

$$P_{CS}(q) = \sum_{i=0}^{N_p} \frac{N}{V} \left[\frac{4\pi}{3} r_i^3 (\rho_{shell}(i) - \rho_{shell}(i+1)) \right]^2 \frac{\sin(qr_i) - qr_i \cos(qr_i)}{(qr_i)^3} \quad (8)$$

In eq. (8), the “shell” number zero refers to the silica core, and the shell number N_p+1 represents the matrix, where N_p is the number of shells outside the silica particle. The last term of the sum, $\rho_{shell}(N_p) - \rho_{shell}(N_p+1)$, is thus the contrast with respect to the matrix. The scattering length density of the matrix is always adjusted such that the total amount of H-chains in the system (and thus equivalently, D-chains), remains constant. This isotopic conservation is the mechanism behind the strong visibility of the silica via its shell leading to the peak at intermediate q although NPs are nominally matched following eq. (5) – see also ¹⁰. A reverse Monte Carlo (RMC) algorithm has been applied to find the best fit under the constraint of a smooth scattering length density profile, following recent work by Cors et al, ⁵⁷ while simultaneously optimizing the size and visibility of the segregated zones as above. The overall fit quality is illustrated in Figure 2 with an adequate description of the peak for both PNCs filled with small and big NPs.

This study has been extended to various chain-mass couples enlarging the matrix asymmetry parameter range from 0.25 to 17. A table summarizing all PNCs investigated here is given in section 4 and the corresponding SANS spectra are given in SI. The fit quality for different values of α highlights the robustness of our approach.

As an outcome of eqs. (7) and (8), segregated zones are present for all matrix asymmetry parameters α , on top of which isotopic shells exist around the NPs for $\alpha > 1$. Two parameters describe the geometry of the segregated zones: their visibility $\Delta\Gamma_H^{seg}$, and their total volume fraction Φ_{seg} deduced from R_{seg} . We have investigated the dependence of both on the matrix asymmetry parameter α in Figure 3. In

Figure 3a, the visibility of the segregated zones is plotted. For $\alpha \leq 1$, it is found to be low and approximately constant (ca. 0.07), whereas it increases significantly for $\alpha > 1$. At the same time, the segregated zones volume fraction Φ_{seg} dominates the matrix volume at $\alpha \leq 1$ in Figure 3b, and decreases to low values ($\approx 5\%$) for $\alpha > 1$. This is accompanied by a decrease of R_{seg} to about 60% of the silica radius. Around $\alpha = 1$, there is a discontinuous jump in Φ_{seg} caused by the “resolution” in α -steps. Note that we have plotted the normalized fractions of polymer with respect to $\Phi_{\text{pol}} = \Phi_{\text{shell}} + \Phi_{\text{seg}} + \Phi_{\text{mat}}$. The reason for the jump is the presence of shells for longer H-chains, which appears to be sudden for the chosen discrete values of the matrix asymmetry. Indeed, the shell volume fraction Φ_{shell} is non-zero only for $\alpha > 1$, and actually prevails in the matrix as can be seen on the right-hand-side of Figure 3b, $\Phi_{\text{shell}} > \Phi_{\text{seg}}$. Thus, the segregated zones are preponderant in volume for PNCs with longer D-chains, but they become smaller – albeit with a higher visibility $|\Delta\Gamma_{\text{H}}^{\text{seg}}|$ – in the opposite case in order to reproduce the intensity of the low-q upturn.

In some sense they are replaced by the shells, i.e., a striking difference in behavior is found for long D- or long H-chains. The segregation is triggered in both cases by the silica NPs, but it is localized close to the silica surface only for long H-chains, with the clear empirical indication of the systematic presence of a peak in the scattered SANS intensity. In spite of the scattering in the data points in Figure 3b, several conclusions can be drawn. There seems to be no tendency with increasing α above 1, i.e., Φ_{shell} appears to remain approximately constant. Secondly, if one changes the particle size as shown in the SI, Φ_{shell} evolves on a slightly lower level (some 15% less), thus remaining within the uncertainty given by the scattering of the data points. The shell volume fraction is thus not sensitive to changes in NP size, in spite of strong variations of the particle number and surface.

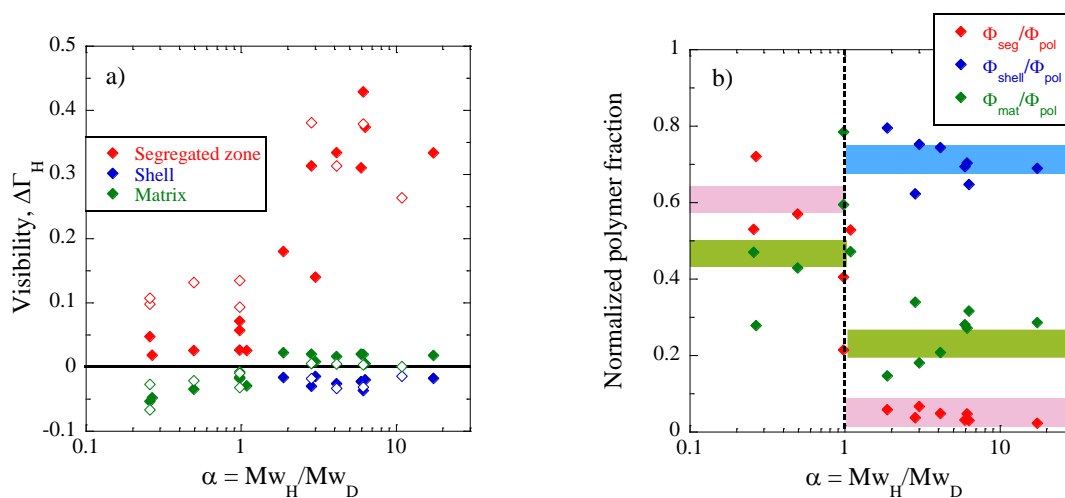


Figure 3. (a) Visibility $\Delta\Gamma_{\text{H}}$ of the segregated zones, shell and matrix, and (b) normalized polymer fractions $\Phi_{\text{shell}}/\Phi_{\text{pol}}$, $\Phi_{\text{mat}}/\Phi_{\text{pol}}$, and $\Phi_{\text{seg}}/\Phi_{\text{pol}}$ as a function of matrix asymmetry parameter. Full and empty symbols are for PNCs filled with small and big NPs, respectively. Colored bars are guides to the eye for the average polymer fractions and their dispersion. The polymer fractions obtained for big NPs are shown in the SI.

Before characterizing in detail the isotopic profile of the shell, we propose a single segregation parameter Θ_{seg} linked to the volume fraction and degree of segregation of the zone, without being sensitive to neither the exact choice of their number density, nor the silica volume fraction:

$$\Theta_{\text{seg}} = |\Delta\Gamma_{\text{H}}^{\text{seg}}| \Phi_{\text{seg}} / \Phi_{\text{NP}} \quad (9)$$

By multiplying the volume and the visibility, this parameter represents the total amount of segregated matter, in analogy with a density. As a conclusion on the bulk segregation behavior of nanocomposites with H/D matrix blends, we have plotted in Figure 4 the segregation parameter Θ_{seg} as a function of matrix asymmetry parameter α . For simplicity, we have named the zones “no shell” and “shell” for $\alpha \leq 1$ and $\alpha > 1$, respectively. The available data points are found to be regrouped around an average value of about 0.15, in spite of the differences in fit parameters and NP sizes. The scattering is indicated by the yellowish zone defined by the standard deviation of the points. This surprising representation suggests that the average quantity of bulk segregation is independent both of silica size and of matrix asymmetry. In other words, if more segregated zones are present, they are less visible, as one could already suspect when comparing Figures 3a and 3b. Also, segregation is triggered by the presence of the silica, and the Θ_{seg} -parameter includes a normalization with respect to the silica volume fraction. The result of data points lying mostly between 0.1 and 0.2 in spite of a variation of the silica content from 4 to 20% (see section 4) implies that the amount of segregated matrix material is proportional to the silica volume fraction.

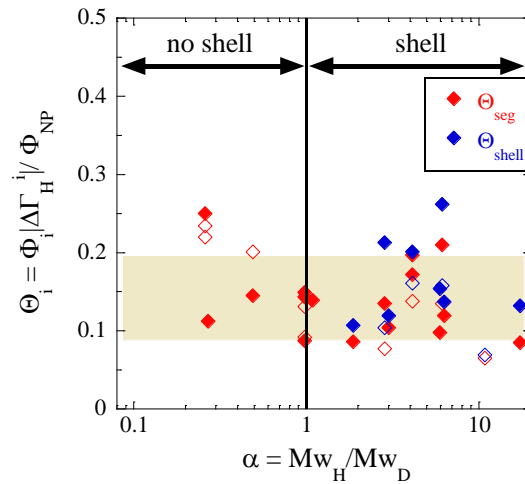


Figure 4. Average degree of H/D segregations Θ_{seg} and Θ_{shell} in PVAc nanocomposites with small (full symbols) and big silica NPs (empty symbols) as indicated in the legend, as a function of matrix asymmetry α .

The same segregation parameter as in eq. (9) can be defined for the shells, based on their average volume fraction and visibility. The result has been superimposed as blue symbols in Figure 4. The data are again quite scattered, but the same order of magnitude as for the bulk segregation is found –

naturally only for $\alpha > 1$, where shells exist. This representation thus underlines the importance of matrix asymmetry: some bulk segregation is always present, but shell segregation is present to the same degree ($\Theta_{\text{shell}} \approx \Theta_{\text{seg}}$), thus doubling the total amount of segregated chain material, only for long H-chains. The isotopic profile $\rho_{\text{shell}}(r)$ has been optimized by RMC in order to provide the best fit, while simultaneously adapting the parameters of the segregated zones for each nanocomposite sample. The resulting fits are decomposed into the different contributions in Figure 5a, and compared to the silica scattering measured in independent SAXS experiments, for small silica NPs (see SI for big NPs).

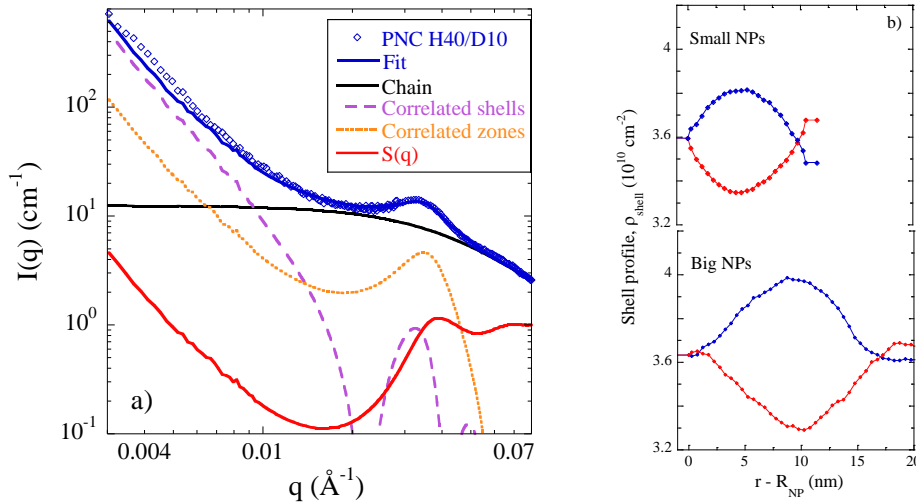


Figure 5. (a) Scattered SANS intensity of asymmetric H40/D10 PNC ($\alpha = 4.1$, $\Phi_{\text{NP}} = 8.7$ %v) compared to the silica structure measured by SAXS of the same sample ($S(q)$, red curve) for small NPs. The blue line is a fit to the SANS data following eq. (7). The purple dashed line and the orange dotted line correspond to the contributions of the contrasted polymer shell and the segregated zones, respectively. Chain scattering is described by RPA using the Debye form factor as described in the text. **(b)** The two solutions (blue and red) of scattering length density profiles within the shell compatible with the scattered SANS intensity, for small NPs (data in a) and big NPs in an equivalent PNC ($\alpha = 4.1$, $\Phi_{\text{NP}} = 9.1$ %v, data in Figure 2b).

The analysis of the different contributions to the total fit in Figure 5a is instructive in several respects. First, it turns out that the peak is not caused by the shell contribution only, although it has some influence (ca. 25% of its value) on the exact peak shape via its form factor oscillation. The peak is caused by the segregated zones, which however need to adjust their radius to small values ($R_{\text{seg}} = 7.2$ nm, in the same range as the silica radius), which leads to the very low volume fraction Φ_{seg} of 4%. Therefore, the amount of segregated polymer material is absolutely insufficient to describe the low- q upturn even if one keeps in mind that the lowest q -values are partially affected by voids or defects. We have checked (see SI) that no satisfying fits of the sharpness of the peak and the low- q behavior can be produced by either neglecting the isotopic shell, or the segregated zones. In order to reproduce the dominant low- q scattering which follows the silica structure factor as shown in Figure 5a, the visibility of the silica gained through the presence of its shell is crucial.

The scattering length density profile within the shell has thus been optimized in order to obtain the best fits of the peak region in shape and intensity. Two examples for profiles around small (resp. big) particles are shown in Figure 5b, as a function of the shifted radius $r - R_{NP}$ starting from the silica surface. The variation of scattering length density is found to extend over ca. 10 nm (resp. 20 nm) for small and big NPs independently of α for $\alpha > 1$ (see SI). The spatial extension of the interfacial layer thus corresponds roughly to half of the interparticle spacing, i.e., a large part of the available space between neighboring NPs, the rest (ca. 25%, resp. 35% for the big NPs – see Figure 3b and SI) being occupied by the matrix. The shape of these profiles is peculiar, if one superimposes the two possible solutions of opposite sign in red and blue with respect to the nominal silica scattering length density, it looks like a fish. The occurrence of two solutions results from the squared contrasts in eqs. (7) and (8). It means that we cannot identify from the SANS analysis which isotopic enrichment (higher H or D concentration with respect to the ZAC condition) takes place in the segregated zones and the shell. It is clear, however, that they have opposite visibility with respect to the matrix. A thermodynamic argument in favor of the preferential adsorption of H-chains is provided below. From a pure scattering point of view, the symmetry of the two opposite profiles of the fish indicates that there is no unsymmetrical contribution like a mass density depletion² close to NPs. In the following, we propose a thermodynamic argument to break the H/D symmetry, arguing that only long H-chains may be enriched at the interface. For the profile, one might have expected a monotonously decaying function starting from the silica surface and progressively approaching the matrix. Note that the latter corresponds to the fish tail by volume conservation, and it is flat by definition of a homogeneous matrix. It will be shown below, though, that a monotonously decaying function can be extracted from the data. Indeed, the exact shape of the scattering length density profile is impacted both by the shape of the segregated regions, and also by the possible geometrical superposition of the segregated zones ($\Phi_{seg} = 4\%$, $R_{seg} = 7.2$ resp. 15.4 nm for small and big NPs) in space with the shells surrounding the silica described by an isotropic model. Concerning fuzziness, it has been varied over a large range as shown in the SI. Good fits are obtained up to 40% of fuzziness, confirming the fish-like shape in all cases.

At this point, one may wonder about thermodynamic equilibrium of the nanocomposites both in terms of spinodal phase decomposition and equilibration of the adsorbed polymer layers.⁵¹ To address this question, we have measured the SANS and SAXS intensities of a selected PNC sample with $\alpha = 6.3$ (see details in Table 2) after annealing under vacuum at increasing temperatures up to 180°C. The SAXS results in Figure 6a clearly show that the filler structure is not modified upon annealing, whereas the SANS intensities in Figure 6b shows only a partial decrease of the low- q upturn – possibly resulting from large-scale reorganization of the voids and defects. In the intermediate q range, the polymer peak remains at the same position, indicating thermodynamically stable polymer shells.

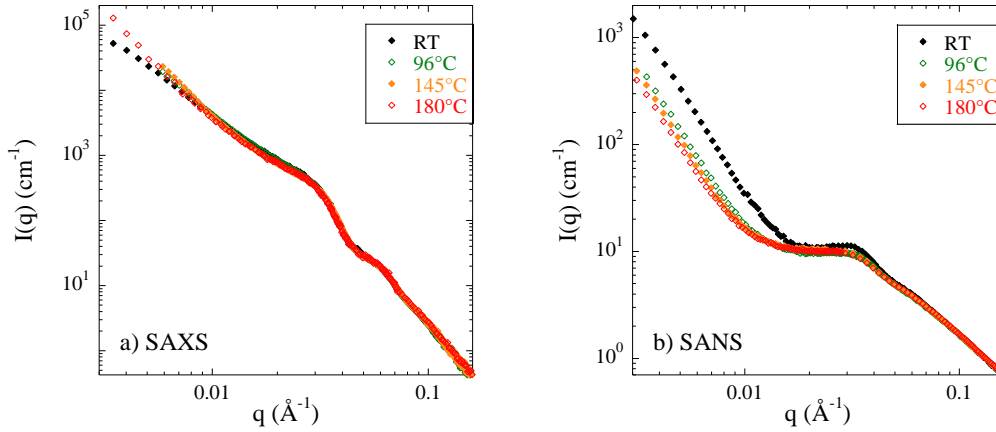


Figure 6. Scattered SAXS **(a)** and SANS **(b)** intensities of PNC with asymmetric blend (H40/D10, $\alpha = 6.3$, $\Phi_{NP} = 8.7\%v$, small NPs) measured at room temperature after consecutive annealing histories: 96°C for 9 days, 145°C for 9 days and an additional 9 hours at 180°C, as indicated in the caption. RT corresponds to the original sample without annealing.

In the graphical abstract, a possible configuration is depicted, with segregated zones overlapping with the profiles close to the silica. Such an interaction is not captured by the isotropic scattering length density profiles, and the model provides an average solution. It is, however, possible to conclude on the exact shape of the profile by analyzing the impact of the geometry on the scattering.

In Figure 7, the idealized situation underlying eq. (7) is illustrated on the left, while the real, crowded situation is shown in the middle. In Figure 7a, both the segregated zones and the silica with its polymer shell are thought to be independently suspended in the matrix, without any overlap. The core-shell form factor of the silica shell is calculated by an angular average over the entire solid angle 4π around the silica NP center, and it thus corresponds to an angularly averaged $\rho(r)$ to be extracted from P_{CS} . In reality, as depicted in Figure 7b, the close presence of the segregated zones due to the crowding necessarily influences the latter average. We will now pursue this idea quantitatively.

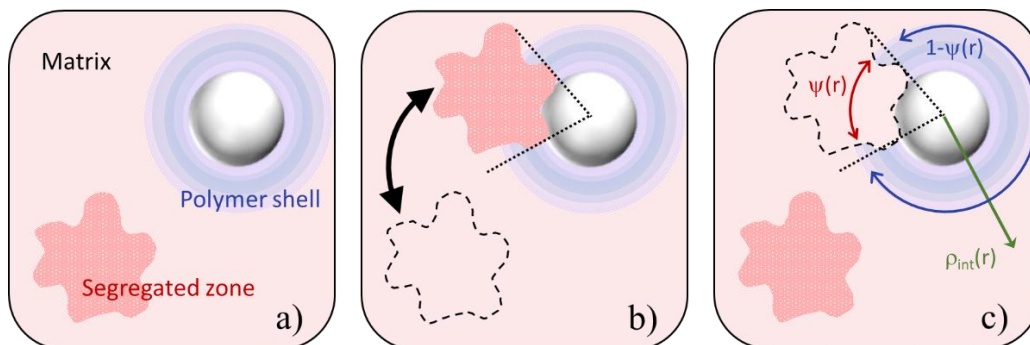


Figure 7. Schematic representation of the ideal **(a)**, real **(b)** and after geometrical transformation **(c)** situations of PNCs with asymmetric ratio $\alpha > 1$ (long H chains, short D chains). In all cases, one can distinguish a segregated zone (dark red) and a silica NP surrounded by an interfacial polymer layer (blue) suspended in the polymer matrix (light red). Colors highlight the different scattering contrasts due to different H/D ratios: blue corresponds to an excess of H and red to an excess of D with respect to the ZAC condition.

The first idea that comes to one's mind when looking at Figure 7b is to simply include the presence of the segregated zones in the angular average. However, this is inconsistent with the conservation of volumes underlying our approach, because in eq. (7) the segregated zones have already been treated independently. Including them in the angular average of the P_{CS} term would thus amount to counting them twice. Maintaining conservation of all volumes, it is possible to pass from the situation in Figure 7b to Figure 7a by moving a segregated zone from the crowded environment "far away" into the matrix as illustrated by the arrow in Figure 7b. This remains consistent with our analysis under the condition that in turn a corresponding piece of matrix is moved to the original position of the segregated zone. The silica with its polymer shell now contains two contributions, the true interfacial profile $\rho_{int}(r)$ in any direction free of segregated zones, and the contribution of the matrix polymer replacing the overlapping segregated zone, as illustrated by the scheme in Figure 7c to reproduce the geometrical constraint shown in Figure 7b. By construction, $\rho_{int}(r)$ is not affected by the segregated zone, but is restricted to a portion of the solid angle. It is thus necessary to replace the 4π -average over a homogeneous environment underlying eq. (7) for P_{CS} by an average over the two contributions. The result is the experimentally observed $\rho(r)$, and it will be possible to deduce the real interfacial profile $\rho_{int}(r)$ by subtraction.

In order to perform this angular average, some geometrical considerations are necessary. First, one needs to estimate the distribution of distances between the silica and its neighboring segregated zones, of number N'_{seg} per NP. It is not possible to access the distance distribution and we have introduced the surface-to-surface distance between the silica NP and the segregated zones, Δ (see SI for details). A negative value of Δ indicates that the polymer of the segregated zones is squeezed onto the silica. In Figure 7c, the volume fraction of the shell occupied by the fuzzy sphere is called $\psi(r)$. A few examples of $\psi(r)$ -functions calculated using a given set of the two free parameters of our model (N'_{seg} and Δ) are shown in SI. We now have the numerical tool to proceed to the angular average. Any spherically symmetric object has a form factor amplitude which reads:

$$F_{CS}(q) = \int_{R_{NP}}^{\infty} \frac{\sin(qr)}{qr} \rho(r) 4\pi r^2 dr \quad (10)$$

where the angular average is performed over a constant and thus produces the $4\pi r^2 dr$ contribution of each volume element, i.e., spherical shells. This is the continuous version of the square given in eq. (8), which had been discretized for numerical purposes. As illustrated in Figure 7c, each shell contains two contributions, one is the matrix scattering length density replacing the segregated zone, ρ_{mat} , and the second one the desired gradient profile, $\rho_{int}(r)$. The volumetric weight of the former is $N'_{seg} \psi(r)$, while the one of the latter is $(1 - N'_{seg} \psi(r))$, where we have directly included the scale-up for several

segregated zones in the vicinity of one silica bead; this remains valid for low N'_{seg} , below their overlap. As a consequence, the average $\rho(r)$ in eq. (10) can be written as the sum of two terms:

$$\rho(r) = N'_{\text{seg}}\psi(r)\rho_{\text{mat}} + \left(1 - N'_{\text{seg}}\psi(r)\right)\rho_{\text{int}}(r) \quad (11)$$

Note that the geometrical transformation described above leads to the replacement of the scattering length density of the segregated zone by ρ_{mat} . As a result, eq. (11) can be solved for the interfacial gradient profile, with the “fish profile” $\rho(r)$ as input. The result depends on the choice of the parameters, N'_{seg} and Δ . The number of neighboring segregated zones is quite directly estimated to 4 ± 2 , because too low numbers do not give any influence as one can guess from the structure of eq. (11), and too high numbers are unphysical due to volume constraints. They also produce unphysical profiles, beyond the maximum possible scattering length densities of pure H or pure D polymer zones. The determination of the second parameter, Δ , is more delicate. As stated above, the position and spatial extension of the fuzzy segregated zone with respect to the silica NP has a direct impact on the range of $\psi(r)$, and thus on the shape of $\rho_{\text{int}}(r)$. We have systematically varied Δ , and analyzed the shape of the resulting interfacial profiles. It results that a continuously decaying profile is found for rather squeezed configurations with Δ values close to $-R_{\text{seg}}$, whereas choices of positive or slightly negative Δ do not improve the profile shape (see Figure S17 in SI). Although there is no a priori argument to exclude any oscillating – fish-like – scattering length density profile, we judge that the physical situation speaks in favor of the simplest gradient. Indeed, the silica surface has been shown to induce the presence of the polymer shell around it, and one spontaneously expects that the influence of the NP surface decays with distance.

We thus conjecture that the simplest solution is also the most physical one: for Δ close to $-R_{\text{seg}}$ and $N'_{\text{seg}} = 4$ to 5, the profiles plotted in Figure 8 are retrieved with eq. (11) for small and big NPs. Due to the contribution proportional to the contrast squared, the SANS analysis itself does not allow concluding about the type of chains (H or D) present at the interface. However, as long chains are entropically more inclined to be localized at surfaces, this suggests that there is an enthalpic preference for H-chains to go to the silica surface, because only in this case of long H-chains the two driving forces do not counteract. As a result of our analysis for each NP size, the interfacial profile has a typical decay range equivalent to the width of the fish, and corresponds to local enrichment of long H-chains on the silica surface, with $\Gamma_{\text{H}} = 75\%$ in volume fraction directly at the surface. Then, the profile decays towards the resulting matrix chain mixture (59.4%H and 40.6%D), which remains close to the ZAC condition. Within error bars, these values are found to be robust for all PNC samples with α above 1.

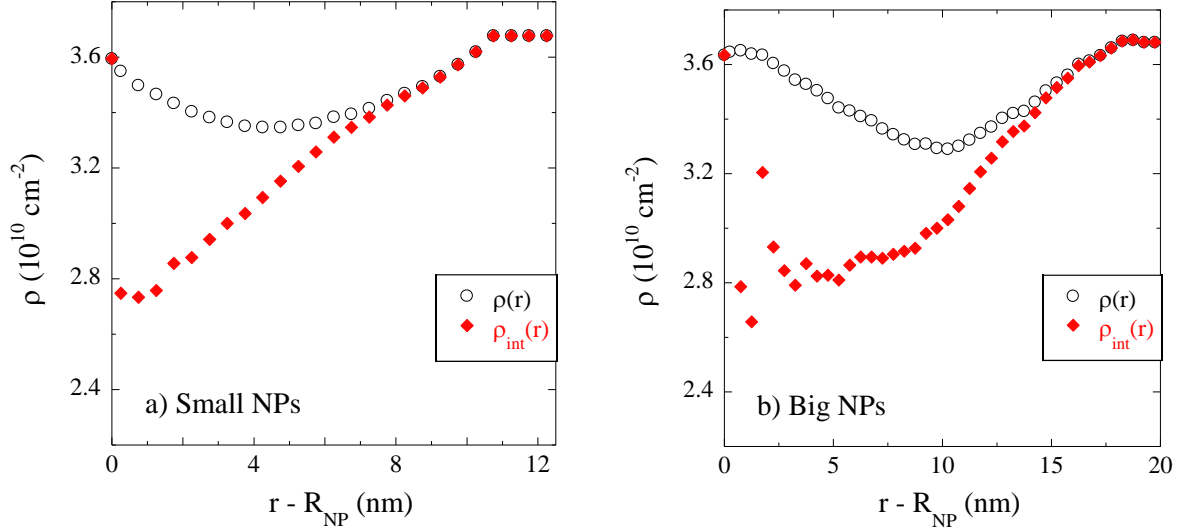


Figure 8. Scattering length density profiles within the shell in asymmetric H40/D10 PNCs ($\alpha = 4.1$) with small **(a)** and big silica NPs **(b)**, $\Phi_{NP} = 8.7$ and 9.1% , respectively. Only the solution with an enrichment in long H chains is represented (circles), and the real interfacial profile (diamonds) is calculated using eq. (11) with $\Delta = 7$ nm, $N'_{seg} = 4$ in **(a)** and $\Delta = 15.2$ nm, $N'_{seg} = 5$ in **(b)**. Δ values are found to be close to $R_{seg} = 7.2$ resp. 15.4 nm for small and big NPs.

This analysis confirms our hypothesis that the spatial extension and relative amplitude expressed by the fish-shaped contrast functions reflect the reality of the unusual isotopic distribution around the NPs. Our model thus extracts in a first time the average picture which includes the overlap with segregated zones, yielding a fish-shape. By then taking the geometry of the zones into account, a monotonously decaying function similar in range is retrieved. It describes the reality of the interface in absence of the perturbation induced by bulk segregation.

CONCLUSIONS

To summarize, we have studied the spatial distribution of PVAc chains of different chain mass in a polymer nanocomposite with attractive silica-polymer interactions. The starting point was to identify any local enrichment of longer or shorter chains close to the nanoparticle surfaces in order to contribute to the understanding of the puzzling dynamics of these systems. The use of H- and D-chains allowed investigating their spatial fluctuations by SANS, under ZAC conditions where the silica NPs are invisible to neutrons. The first surprising result of our study is that while chains mix at a molecular level in all situations studied here, they do present spatial fluctuations of two different types in PNCs, depending on the matrix asymmetry. In all cases, bulk segregation is found and quantitatively described – we underline that this is virtually never done in the literature where low- q upturns are usually discarded, although it is also found in theoretical work and compared to SAXS experiments,

which however do not resolve chain structure.⁴⁸ The total amount of bulk segregation is found to remain roughly constant. In terms of the phase diagram of such complex polymer and NP blends, we interpret this as the signature of an approach of the spinodal phase separation line of the H/D system caused by the ternary interaction with the silica NPs. This creates metastable H/D concentration fluctuations which however are quenched in the process of solvent evaporation.

Even more surprisingly, in the case of the long H-chains, an additional interfacial segregation mechanism is evidenced by a clear sign in the scattered intensity, a peak located in the silica-size range, which moves as the silica size is changed. Note that this feature is robust with changes to both H and D chain masses keeping $\alpha > 1$, as shown by the many examples in the SI. As the silica itself remains unchanged, this must be due to a modification of the isotopic density close to the NPs. We have thus enlarged our scattering model to accommodate also the contribution of an isotopic shell, while of course maintaining bulk segregation and volume conservation of all isotopes throughout the sample. As a result, shell scattering is described by a scattering length density profile around the NPs with a peculiar, fish-like geometry. From all our attempts to describe this profile in different manners, it results that such a profile must be present to describe the data. We have then shown that the geometric detail of the fish-profile can be explained by the superposition with anisotropic contributions. The latter stem from the segregated globular zones which are present in all samples (Figure 7). Taking into account the geometrical superposition allows extracting the purely interfacial gradient, i.e., not affected by the segregated zones. The corresponding decay is found to extend over ca. 10 – 20 nm into the bulk, and amounts to a local enrichment of ca. 75% in H-chains, as compared to the average matrix value of 60%.

To summarize, there is thus strong evidence for an isotopic (H) enrichment close to the NP surfaces in presence of long H-chains, which combine entropic and enthalpic preference for the silica. This mechanism results in an overall stronger segregation because it adds interfacial segregation to the bulk one. The silica thus destabilizes the H/D mixture, inducing different types of segregation depending on the chain mass asymmetry. As a conclusion, a surprising variety of spatial segregation phenomena is triggered by the combination of particle surfaces, chain mass, and isotopic differences in such systems. On the other hand, the chain conformations themselves do not seem to be impacted, suggesting that although chains have a tendency to separate, they are locally mixed and at equilibrium at small scales. Combining knowledge of the present spatial distribution with comparative studies of dynamic properties of isotopically labeled systems with pure hydrogenated systems may thus finally enable molecular understanding of the striking dynamic properties of PNCs with attractive interactions towards the particles.

EXPERIMENTAL SECTION

Materials. Hydrogenated and deuterated poly(vinyl acetate)s of different chain mass ranging from ca 10 up to 110 kg/mol were synthesized via reversible addition–fragmentation chain transfer (RAFT) polymerization. All details are given in ². H240 in Table 1 is a commercial product from Scientific Polymer Product Inc. Molecular weights were obtained by SEC at 25 °C in THF (Agilent 1310B 1260 Infinity Isocratic HPLC). Two different batches of spherical silica NPs were synthesized by a modified Stöber method ⁵⁸ in ethanol where they are electrostatically stabilized, with a final NP concentration of 16 mg/mL. They have been characterized by SAXS in ethanol at 0.3 vol % dilution. For each batch, the scattered intensity revealed a log-normal size distribution with an average NP radius of 9.5 and 21.3 nm for the small and big NPs, respectively (see the SI for details).

PNC formulation. The hydrogenated and deuterated polymers dissolved in MEK were mixed with the proportions calculated to obtain a nominal silica content of 9 vol % in the final PNCs. In some cases, the silica content was varied to cover a range of concentrations from ca. 4 to 20%v. All samples were prepared using the H/D volume fraction ratio of PVAc necessary to fulfill the ZAC condition (ca. 60/40, see SI for details). After 12 h of mixing, the solvent was evaporated by progressive casting over 1 day, thus forming nanocomposites. The procedure was completed by 3 days under vacuum at room temperature. Exact PNC loadings were determined by thermogravimetric analysis (TA Discovery, 20 °C/min, under air) from the weight loss between 200 and 900 °C. The silica volume fraction, Φ_{NP} , was determined by mass conservation using the densities of neat PVAc and silica, 1.25 and 2.22 g/cm³, respectively. All the PNC samples studied are described in Table 2.

Table 2. PNC samples characteristics

| Silica size | α | Mw _H (kg/mol) | Mw _D (kg/mol) | Φ_{NP} (%v) |
|-------------|----------|--------------------------|--------------------------|------------------|
| Small NPs | 0.26 | 10.2 | 39.6 | 9.2 |
| | 0.27 | 10.6 | 39.6 | 10.6 |
| | 0.49 | 19.6 | 39.6 | 9.3 |
| | 0.98 | 10.2 | 10.4 | 4.3 |
| | 0.98 | 10.2 | 10.4 | 6.9 |
| | 0.98 | 10.2 | 10.4 | 12.4 |
| | 1.09 | 43 | 39.6 | 9.0 |
| | 1.88 | 19.6 | 10.4 | 10.8 |
| | 2.85 | 113 | 39.6 | 8.0 |
| | 3.02 | 19.6 | 6.5 | 8.3 |
| | 4.13 | 43.0 | 10.4 | 8.7 |
| | 5.95 | 38.7 | 6.5 | 9.1 |
| | 6.13 | 242.7 | 39.6 | 8.8 |
| | 6.31 | 41 | 6.5 | 8.7 |
| 17.38 | 113 | 6.5 | 8.3 | |

| | | | | |
|---------|-------|-------|------|------|
| Big NPs | 0.26 | 10.2 | 39.6 | 8.3 |
| | 0.26 | 10.2 | 39.6 | 15.7 |
| | 0.49 | 19.6 | 39.6 | 8.4 |
| | 0.98 | 10.2 | 10.4 | 6.4 |
| | 0.98 | 10.2 | 10.4 | 20.6 |
| | 2.85 | 113 | 39.6 | 8.0 |
| | 4.13 | 43 | 10.4 | 9.1 |
| | 6.13 | 242.7 | 39.6 | 8.9 |
| | 10.87 | 113 | 10.4 | 8.9 |

Structural Analysis. SAXS experiments were performed using an in-house setup of the Laboratoire Charles Coulomb, “Réseau X et gamma”, University of Montpellier, France. A high-brightness low-power X-ray tube, coupled with aspheric multilayer optics (GeniX3D from Xenocs), was employed. The scattered intensities were measured by a two dimensional “Pilatus” pixel detector at a sample-to-detector distance $D = 1.9$ m, leading to a q range from 5.5×10^{-3} to 0.2 \AA^{-1} . To extend the q -range, additional SAXS experiments were conducted on beamline ID02⁵⁹ at the European Synchrotron Radiation Facility (ESRF, Grenoble FR) at a wavelength of 1 \AA with $D = 30.7$ m, yielding a low- q value of $2.3 \times 10^{-4} \text{ \AA}^{-1}$. The scattering cross section per unit sample volume $d\Sigma/d\Omega$ (in cm^{-1}), which we term scattered intensity $I(q)$, was obtained by using standard procedures including background subtraction and calibration.⁸ SANS experiments were performed on D11 at the Institut Laue-Langevin (ILL, Grenoble FR) using different configurations covering a q -range from 3×10^{-3} to 0.6 \AA^{-1} : $D = 24$ m; $D = 8$ m; and $D = 1.4$ m, all with a wavelength of 4.6 \AA . Samples with a thickness of ca. 0.12 mm were mounted between two quartz windows. Empty cell subtraction, calibration by 1 mm light water in Hellma cuvette, and absolute determination of scattering cross sections $I(q)$ were performed using standard procedures. The reduction of raw data including corrections for detector sensitivity and background noise was performed by the program Lamp.⁶⁰ In all cases, the same piece of sample was used for both SAXS and SANS measurements.

ACKNOWLEDGMENTS

This work was supported by the U.S. Department of Energy, Office of Science, Basic Energy Sciences, Materials Sciences and Engineering Division. A.-C.G. and J.O. are thankful for support by the ANR NANODYN project, Grant ANR-14-CE22-0001-01 of the French Agence Nationale de la Recherche. The authors thank the Institut Laue-Langevin (ILL) for supplying beam-time under the proposal number 9-12-505.⁶¹ The low- q SAXS experiments were performed on beamline ID02 at the European Synchrotron Radiation Facility (ESRF), Grenoble, France. We are grateful to Michael Sztucki at the ESRF for providing assistance in using beamline ID02.

Supporting Information. Complementary SANS and SAXS data, details of the fuzzy form factor, full characteristics of the segregated zones, and additional details on the modeling of the interfacial segregation.

REFERENCES

- (1) Füllbrandt, M.; Purohit, P. J.; Schönhals, A., Combined Ftir and Dielectric Investigation of Poly(Vinyl Acetate) Adsorbed on Silica Particles. *Macromolecules* **2013**, *46* (11), 4626-4632.
- (2) Genix, A.-C.; Bocharova, V.; Carroll, B.; Lehmann, M.; Saito, T.; Krueger, S.; He, L.; Dieudonné-George, P.; Sokolov, A. P.; Oberdisse, J., Understanding the Static Interfacial Polymer Layer by Exploring the Dispersion States of Nanocomposites. *ACS Applied Materials & Interfaces* **2019**, *11* (19), 17863-17872.
- (3) Cheng, S.; Carroll, B.; Bocharova, V.; Carrillo, J.-M.; Sumpter, B. G.; Sokolov, A. P., Focus: Structure and Dynamics of the Interfacial Layer in Polymer Nanocomposites with Attractive Interactions. *J. Chem. Phys.* **2017**, *146* (20), 203201.
- (4) Carroll, B.; Cheng, S.; Sokolov, A. P., Analyzing the Interfacial Layer Properties in Polymer Nanocomposites by Broadband Dielectric Spectroscopy. *Macromolecules* **2017**, *50* (16), 6149-6163.
- (5) Musino, D.; Oberdisse, J.; Farago, B.; Alegria, A.; Genix, A.-C., Resolving Segmental Polymer Dynamics in Nanocomposites by Incoherent Neutron Spin–Echo Spectroscopy. *ACS Macro Letters* **2020**, *9* (6), 910-916.
- (6) Baeza, G. P.; Oberdisse, J.; Alegria, A.; Saalwaechter, K.; Couty, M.; Genix, A.-C., Depercolation of Aggregates Upon Polymer Grafting in Simplified Industrial Nanocomposites Studied with Dielectric Spectroscopy. *Polymer* **2015**, *73*, 131-138.
- (7) Mujtaba, A.; Keller, M.; Ilisch, S.; Radusch, H. J.; Beiner, M.; Thurn-Albrecht, T.; Saalwächter, K., Detection of Surface-Immobilized Components and Their Role in Viscoelastic Reinforcement of Rubber–Silica Nanocomposites. *ACS Macro Letters* **2014**, *3* (5), 481-485.
- (8) Lindner, P.; Zemb, T., *Neutrons, X-Ray and Light Scattering*. North Holland, Elsevier: Amsterdam, 2002.
- (9) Cotton, J. P.; Decker, D.; Benoit, H.; Farnoux, B.; Higgins, J.; Jannink, G.; Ober, R.; Picot, C.; Cloizeau, J. D., Conformation of Polymer-Chain in Bulk. *Macromolecules* **1974**, *7* (6), 863-872.
- (10) Banc, A.; Genix, A. C.; Dupas, C.; Sztucki, M.; Schweins, R.; Appavou, M. S.; Oberdisse, J., On the Origin of Small-Angle Scattering from Contrast-Matched Nanoparticles: A Study of Chain and Filler Structure in Polymer Nanocomposites. *Macromolecules* **2015**, *48* (18), 6596–6605.

- (11) Jouault, N.; Dalmás, F.; Said, S.; Di Cola, E.; Schweins, R.; Jestin, J.; Boué, F., Direct Measurement of Polymer Chain Conformation in Well-Controlled Model Nanocomposites by Combining Sans and Saxes. *Macromolecules* **2010**, *43* (23), 9881-9891.
- (12) Cotton, J. P., Variations on Contrast in Sans: Determination of Self and Distinct Correlation Functions. *Adv. Colloid Interface Sci.* **1996**, *69*, 1-29.
- (13) Flory, P. J., *Principles of Polymer Chemistry*. Cornell University Press: 1953.
- (14) de Gennes, P.-G., *Scaling Concepts in Polymer Physics*. Cornell University Press: Ithaca, 1979.
- (15) Shibayama, M.; Stein, R. S.; Han, C. C., Study of Miscibility and Critical Phenomena of Deuterated Polystyrene and Hydrogenated Poly(Vinyl Methyl Ether) by Small-Angle Neutron Scattering. *Macromolecules* **1985**, *18* (11), 2179-2187.
- (16) Strobl, G. R., *The Physics of Polymers* Springer-Verlag Berlin Heidelberg: 2007.
- (17) Binder, K., Phase Transitions in Polymer Blends and Block Copolymer Melts: Some Recent Developments. In *Theories and Mechanism of Phase Transitions, Heterophase Polymerizations, Homopolymerization, Addition Polymerization*, Springer Berlin Heidelberg: Berlin, Heidelberg, 1994; pp 181-299.
- (18) Holyst, R.; Vilgis, T. A., The Structure and Phase Transitions in Polymer Blends, Diblock Copolymers and Liquid Crystalline Polymers: The Landau-Ginzburg Approach. *Macromolecular Theory and Simulations* **1996**, *5* (4), 573-643.
- (19) Cahn, J. W.; Hilliard, J. E., Free Energy of a Nonuniform System. I. Interfacial Free Energy. *The Journal of chemical physics* **1958**, *28* (2), 258-267.
- (20) Nishi, T.; Wang, T. T.; Kwei, T. K., Thermally Induced Phase Separation Behavior of Compatible Polymer Mixtures. *Macromolecules* **1975**, *8* (2), 227-234.
- (21) Yasuda, O.; Ougizawa, T.; Inoue, T.; Miyasaka, K., Formation of Regular Two-Phase Structure During Solution Casting of a Polymer Blend. *Journal of Polymer Science: Polymer Letters Edition* **1983**, *21* (10), 813-818.
- (22) Higgins, J. S.; Cabral, J. T., A Thorny Problem? Spinodal Decomposition in Polymer Blends. *Macromolecules* **2020**, *53* (11), 4137-4140.
- (23) Inoue, T.; Ougizawa, T.; Yasuda, O.; Miyasaka, K., Development of Modulated Structure During Solution Casting of Polymer Blends. *Macromolecules* **1985**, *18* (1), 57-63.
- (24) Janssen, S.; Schwahn, D.; Springer, T., Mean-Field Ising Crossover and the Critical Exponents Gamma, Nu, and Eta for a Polymer Blend: D-Pb/Ps Studied by Small-Angle Neutron Scattering. *Physical Review Letters* **1992**, *68* (21), 3180-3183.
- (25) Schwahn, D.; Mortensen, K.; Yee-Madeira, H., Mean-Field and Ising Critical Behavior of a Polymer Blend. *Physical Review Letters* **1987**, *58* (15), 1544-1546.

- (26) Ginzburg, V. V., Influence of Nanoparticles on Miscibility of Polymer Blends. A Simple Theory. *Macromolecules* **2005**, *38* (6), 2362-2367.
- (27) Taguet, A.; Cassagnau, P.; Lopez-Cuesta, J. M., Structuration, Selective Dispersion and Compatibilizing Effect of (Nano)Fillers in Polymer Blends. *Progress in Polymer Science* **2014**, *39* (8), 1526-1563.
- (28) He, G.; Ginzburg, V. V.; Balazs, A. C., Determining the Phase Behavior of Nanoparticle-Filled Binary Blends. *Journal of Polymer Science Part B: Polymer Physics* **2006**, *44* (17), 2389-2403.
- (29) Nesterov, A. E.; Lipatov, Y. S., Compatibilizing Effect of a Filler in Binary Polymer Mixtures. *Polymer* **1999**, *40* (5), 1347-1349.
- (30) Chung, H. J.; Taubert, A.; Deshmukh, R. D.; Composto, R. J., Mobile Nanoparticles and Their Effect on Phase Separation Dynamics in Thin-Film Polymer Blends. *Europhysics Letters (EPL)* **2004**, *68* (2), 219-225.
- (31) Balazs, A. C.; Emrick, T.; Russell, T. P., Nanoparticle Polymer Composites: Where Two Small Worlds Meet. *Science* **2006**, *314* (5802), 1107-1110.
- (32) Maguire, S. M.; Krook, N. M.; Kulshreshtha, A.; Bilchak, C. R.; Brosnan, R.; Pana, A.-M.; Rannou, P.; Maréchal, M.; Ohno, K.; Jayaraman, A.; Composto, R. J., Interfacial Compatibilization in Ternary Polymer Nanocomposites: Comparing Theory and Experiments. *Macromolecules* **2021**, *54* (2), 797-811.
- (33) Cheng, S. W.; Holt, A. P.; Wang, H. Q.; Fan, F.; Bocharova, V.; Martin, H.; Etampawala, T.; White, B. T.; Saito, T.; Kang, N. G.; Dadmun, M. D.; Mays, J. W.; Sokolov, A. P., Unexpected Molecular Weight Effect in Polymer Nanocomposites. *Physical Review Letters* **2016**, *116* (3).
- (34) Genix, A.-C.; Bocharova, V.; Kisliuk, A.; Carroll, B.; Zhao, S.; Oberdisse, J.; Sokolov, A. P., Enhancing the Mechanical Properties of Glassy Nanocomposites by Tuning Polymer Molecular Weight. *ACS Applied Materials & Interfaces* **2018**, *10* (39), 33601-33610.
- (35) Bocharova, V.; Genix, A.-C.; Carrillo, J.-M. Y.; Kumar, R.; Carroll, B.; Erwin, A.; Voylov, D.; Kisliuk, A.; Wang, Y.; Sumpter, B. G.; Sokolov, A. P., Addition of Short Polymer Chains Mechanically Reinforces Glassy Poly(2-Vinylpyridine)-Silica Nanoparticle Nanocomposites. *ACS Applied Nano Materials* **2020**, *3* (4), 3427-3438.
- (36) Oh, S. M.; Abbasi, M.; Shin, T. J.; Saalwächter, K.; Kim, S. Y., Initial Solvent-Driven Nonequilibrium Effect on Structure, Properties, and Dynamics of Polymer Nanocomposites. *Physical Review Letters* **2019**, *123* (16), 167801.
- (37) Ramzi, A.; Zielinski, F.; Bastide, J.; Boue, F., Butterfly Patterns: Small-Angle Neutron Scattering from Deuterated Mobile Chains in a Randomly Cross-Linked Polystyrene Network. *Macromolecules* **1995**, *28* (10), 3570-3587.

- (38) Nowicki, W., Structure and Entropy of a Long Polymer Chain in the Presence of Nanoparticles. *Macromolecules* **2002**, *35* (4), 1424-1436.
- (39) White, R. P.; Lipson, J. E. G.; Higgins, J. S., Effect of Deuterium Substitution on the Physical Properties of Polymer Melts and Blends. *Macromolecules* **2010**, *43* (9), 4287-4293.
- (40) Bates, F. S.; Wiltzius, P., Spinodal Decomposition of a Symmetric Critical Mixture of Deuterated and Protonated Polymer. *The Journal of chemical physics* **1989**, *91* (5), 3258-3274.
- (41) Bates, F. S.; Wignall, G. D.; Koehler, W. C., Critical-Behavior of Binary-Liquid Mixtures of Deuterated and Protonated Polymers. *Physical Review Letters* **1985**, *55* (22), 2425-2428.
- (42) Jones, R. A. L.; Norton, L. J.; Kramer, E. J.; Bates, F. S.; Wiltzius, P., Surface-Directed Spinodal Decomposition. *Phys Rev Lett* **1991**, *66* (10), 1326-1329.
- (43) Jones, R. A. L.; Kramer, E. J.; Rafailovich, M. H.; Sokolov, J.; Schwarz, S. A., Surface Enrichment in an Isotopic Polymer Blend. *Phys Rev Lett* **1989**, *62* (3), 280-283.
- (44) Geoghegan, M.; Nicolai, T.; Penfold, J.; Jones, R. A. L., Kinetics of Surface Segregation and the Approach to Wetting in an Isotopic Polymer Blend. *Macromolecules* **1997**, *30* (14), 4220-4227.
- (45) Hariharan, A.; Kumar, S. K.; Russell, T. P., Reversal of the Isotopic Effect in the Surface Behavior of Binary Polymer Blends. *J. Chem. Phys.* **1993**, *98* (5), 4163-4173.
- (46) Hariharan, A.; Kumar, S. K.; Russell, T. P., Free Surfaces of Polymer Blends. II. Effects of Molecular Weight and Applications to Asymmetric Polymer Blends. *J. Chem. Phys.* **1993**, *99* (5), 4041-4050.
- (47) Crawford, M. K.; Smalley, R. J.; Cohen, G.; Hogan, B.; Wood, B.; Kumar, S. K.; Melnichenko, Y. B.; He, L.; Guise, W.; Hammouda, B., Chain Conformation in Polymer Nanocomposites with Uniformly Dispersed Nanoparticles. *Physical Review Letters* **2013**, *110* (19), 196001.
- (48) Zhou, Y.; Yavitt, B. M.; Zhou, Z.; Bocharova, V.; Salatto, D.; Endoh, M. K.; Ribbe, A. E.; Sokolov, A. P.; Koga, T.; Schweizer, K. S., Bridging-Controlled Network Microstructure and Long-Wavelength Fluctuations in Silica–Poly(2-Vinylpyridine) Nanocomposites: Experimental Results and Theoretical Analysis. *Macromolecules* **2020**, *53* (16), 6984-6994.
- (49) Hooper, J. B.; Schweizer, K. S., Real Space Structure and Scattering Patterns of Model Polymer Nanocomposites. *Macromolecules* **2007**, *40* (19), 6998-7008.
- (50) Kim, S. Y.; Schweizer, K. S.; Zukoski, C. F., Multiscale Structure, Interfacial Cohesion, Adsorbed Layers, and Thermodynamics in Dense Polymer-Nanoparticle Mixtures. *Phys Rev Lett* **2011**, *107* (22), 225504.
- (51) Hall, L. M.; Schweizer, K. S., Many Body Effects on the Phase Separation and Structure of Dense Polymer-Particle Melts. *J. Chem. Phys.* **2008**, *128* (23), 234901.
- (52) Benoit, H. C.; Higgins, J. S., *Polymers and Neutron Scattering*. Oxford University Press: Oxford, 1994.

- (53) Tung, W.-S.; Bird, V.; Composto, R. J.; Clarke, N.; Winey, K. I., Polymer Chain Conformations in Cnt/Ps Nanocomposites from Small Angle Neutron Scattering. *Macromolecules* **2013**, *46* (13), 5345-5354.
- (54) Hall, L. M.; Anderson, B. J.; Zukoski, C. F.; Schweizer, K. S., Concentration Fluctuations, Local Order, and the Collective Structure of Polymer Nanocomposites. *Macromolecules* **2009**, *42* (21), 8435-8442.
- (55) Sen, S.; Xie, Y.; Kumar, S. K.; Yang, H.; Bansal, A.; Ho, D. L.; Hall, L.; Hooper, J. B.; Schweizer, K. S., Chain Conformations and Bound-Layer Correlations in Polymer Nanocomposites. *Phys Rev Lett* **2007**, *98* (12), 128302.
- (56) Shimizu, R.; Tanaka, H., Impact of Complex Topology of Porous Media on Phase Separation of Binary Mixtures. *Science Advances* **2017**, *3* (12), eaap9570.
- (57) Cors, M.; Wiehemeier, L.; Wrede, O.; Feoktystov, A.; Cousin, F.; Hellweg, T.; Oberdisse, J., Contrast Variation Sans Measurement of Shell Monomer Density Profiles of Smart Core–Shell Microgels. *Soft Matter* **2020**, *16* (7), 1922-1930.
- (58) Hidehiro, K.; Hisao, S.; Daisuke, K.; Genji, J., Densification of Alkoxide-Derived Fine Silica Powder Compact by Ultra-High-Pressure Cold Isostatic Pressing. *Journal of the American Ceramic Society* **1993**, *76* (1), 54-64.
- (59) Narayanan, T.; Sztucki, M.; Van Vaerenbergh, P.; Leonardon, J.; Gorini, J.; Claustre, L.; Sever, F.; Morse, J.; Boesecke, P., A Multipurpose Instrument for Time-Resolved Ultra-Small-Angle and Coherent X-Ray Scattering. *J. Appl. Cryst.* **2018**, *51* (6), 1511-1524.
- (60) Richard, D.; Ferrand, M.; Kearley, G. J., Analysis and Visualisation of Neutron-Scattering Data. *Journal of Neutron Research* **1996**, *4* (1-4), 33-39.
- (61) Genix, A. C.; Carroll, B.; Chauveau, E.; Oberdisse, J.; Schweins, R.; Sokolov, A. P., Characterization of the Depleted Interfacial Layer and Chain Desorption in Polymer Nanocomposites by Sans Using Numerical Simulations. Institut Laue-Langevin (ILL) Doi:10.5291/ILL-Data.9-12-505 **2018**.